AD-A066 976 SRI INTERNATIONAL MENLO PARK CA F/G 17/9
RELATIVE INTENSITY OF INCOHERENT AND SEMICOHERENT SCATTERING FR--ETC(U)
JUL 78 W G CHESNUT DNA001-78-C-0075
UNCLASSIFIED DNA-4666T NL

| OF |
AD A066976

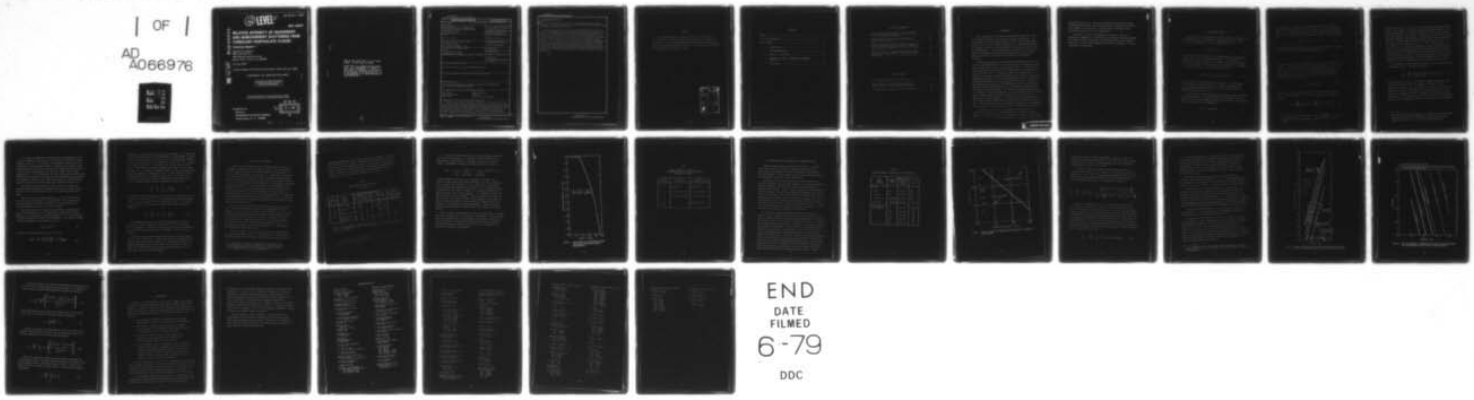

END
DATE FILMED
6-79
DDC

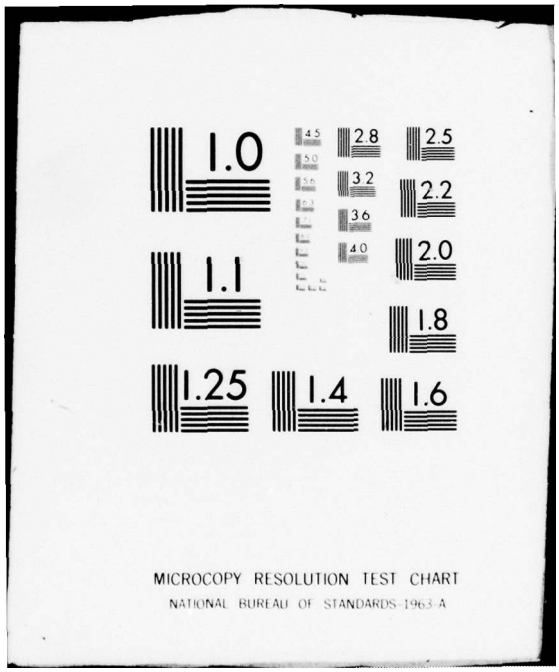
1.0
1.1
1.25
1.4
1.6
1.8
2.0
2.2
2.5
2.8
3.2
3.6
4.0
4.5
5.0
5.6
MICROCOPY RESOLUTION TEST CHART
NATIONAL BUREAU OF STANDARDS-1963-A

(12) LEVEL III

DNA 4666T

RELATIVE INTENSITY OF INCOHERENT AND SEMICOHERENT SCATTERING FROM TURBULENT PARTICULATE CLOUDS

Technical Report 1

Walter G. Chesnut
SRI International
333 Ravenswood Avenue
Menlo Park, California 94025

31 July 1978

Topical Report for Period 21 November 1977—31 July 1978

CONTRACT No. DNA 001-78-C-0075

APPROVED FOR PUBLIC RELEASE;
DISTRIBUTION UNLIMITED.

THIS WORK SPONSORED BY THE DEFENSE NUCLEAR AGENCY
UNDER RDT&E RMSS CODE B322078464 S99QAXHB05414 H2590D.

Prepared for
Director
DEFENSE NUCLEAR AGENCY
Washington, D. C. 20305

Destroy this report when it is no longer needed. Do not return to sender.

PLEASE NOTIFY THE DEFENSE NUCLEAR AGENCY, ATTN: TISI, WASHINGTON, D.C. 20305, IF YOUR ADDRESS IS INCORRECT, IF YOU WISH TO BE DELETED FROM THE DISTRIBUTION LIST, OR IF THE ADDRESSEE IS NO LONGER EMPLOYED BY YOUR ORGANIZATION.

UNCLASSIFIED

SECURITY CLASSIFICATION OF THIS PAGE (When Data Entered)

REPORT DOCUMENTATION PAGE		READ INSTRUCTIONS BEFORE COMPLETING FORM
1. REPORT NUMBER DNA 4666T	2. GOVT ACCESSION NO.	3. RECIPIENT'S CATALOG NUMBER
4. TITLE (and Subtitle) RELATIVE INTENSITY OF INCOHERENT AND SEMICOHERENT SCATTERING FROM TURBULENT PARTICULATE CLOUDS Technical Report 1		5. TYPE OF REPORT & PERIOD COVERED Topical Report for Period 21 Nov 77—31 July 78 6. PERFORMING ORG. REPORT NUMBER SRI Project 6990
7. AUTHOR(s) Walter G. Chesnut		8. CONTRACT OR GRANT NUMBER(s) DNA 001-78-C-0075
9. PERFORMING ORGANIZATION NAME AND ADDRESS SRI International 333 Ravenswood Avenue Menlo Park, California 94025		10. PROGRAM ELEMENT, PROJECT, TASK AREA & WORK UNIT NUMBERS Subtask S99QAXHB054-14
11. CONTROLLING OFFICE NAME AND ADDRESS Director Defense Nuclear Agency Washington, D.C. 20305		12. REPORT DATE 31 July 1978 13. NUMBER OF PAGES 32
14. MONITORING AGENCY NAME & ADDRESS(if different from Controlling Office)		15. SECURITY CLASS (of this report) UNCLASSIFIED 15a. DECLASSIFICATION DOWNGRADING SCHEDULE

16. DISTRIBUTION STATEMENT (of this Report)

Approved for public release; distribution unlimited.

17. DISTRIBUTION STATEMENT (of the abstract entered in Block 20, if different from Report)

18. SUPPLEMENTARY NOTES

This work sponsored by the Defense Nuclear Agency under RDT&E RMSS Code B322078464 S99QAXHB05414 H2590D.

19. KEY WORDS (Continue on reverse side if necessary and identify by block number)

Nuclear Dust	Radar Scattering
High Explosive Dust	Turbulence
Dust Clouds	Particle Size Distribution

20. ABSTRACT (Continue on reverse side if necessary and identify by block number)

Recently, interest has revived in the nature of radar backscatter from dust clouds lofted by surface nuclear detonations. As a result, radar backscatter experiments are being performed on high-explosive-produced dust clouds. Traditionally, the measurements obtained are interpreted as being the result of incoherent addition of scattering from the individual dust particles. However, during their early stages of evolution, such clouds demonstrate intense turbulence with apparent abrupt transitions from clean to dirty air.

OVER

DD FORM 1 JAN 73 1473 EDITION OF 1 NOV 65 IS OBSOLETE

UNCLASSIFIED

SECURITY CLASSIFICATION OF THIS PAGE (When Data Entered)

20. ABSTRACT (Continued)

Such an environment seems conductive to contributions from semicoherent scattering. If such coherent contributions are important, then data interpretation must consider this process.

This document presents analytical scattering formulas to be used to compare the magnitude of the two scattering processes, incoherent and semicoherent. A plausible model of the in-situ, three-dimensional spatial frequency power spectrum of dielectric fluctuations in the dust/air interface is presented, and an analytical model of the dust-particle size distribution is derived--based loosely on the sketchy field measurement data available to us. Finally, all of the pieces of our analytical formalisms are assembled. The results show that the semicoherent scattering contribution to radar backscattering from high-explosive-produced dust clouds is very likely significantly weaker than contributions from incoherent scattering. We conclude that interpretation of radar backscatter data--for example, that of the Miser's Bluff radar experiments--need not consider coherent scattering processes.

PREFACE

The author thanks two of his associates, Dr. Joseph Depp and Dr. Alan Burns, for numerous stimulating discussions. Dr. Burns and Dr. Depp are currently performing radar and lidar (laser radar) measurements of backscatter energy from the Miser's Bluff detonations performed by DNA during June and August of 1978.

CONTENTS

LIST OF ILLUSTRATIONS

LIST OF TABLES

1. INTRODUCTION

Radar signals may be scattered from particulate clouds (e.g. dust, water droplets, aerosols, free electrons) through two processes. The first process is the incoherent addition of power from each individual particle. We call this incoherent scattering. If the particulate cloud is nonuniform in density, then semicoherent scattering may result from the irregularities. In some environments, specifically in free electron plasmas, semicoherent scattering from irregularities in the electron plasma may be 10^6 to 10^{10} times more intense than the incoherent scattering.

Scattering measurements in high-explosive-produced dust clouds, the subject of principal concern here, have always been interpreted as though the scattering were due only to the incoherent process. The question of whether coherent scattering effects can contribute to the measured radar returns has been raised. To shed some light on this possibility, we present in this document analytical formalisms that allow us to relate the comparative intensity of the two scattering phenomenon to the particulate environmental properties of explosive-produced dust clouds. Finally, we make quantitative estimates of the contributions of the two processes to determine whether radar backscatter data interpretation should consider the coherent scattering process. Since the two scattering processes have very different frequency dependencies, it was also thought that the analysis might provide insight into another technique that could be useful in diagnosing dust cloud properties. As we shall show, for likely models of dust clouds, coherent backscattering (radar mode) is probably not significant. This then indicates that the frequency dependence of multifrequency radar backscatter data is directly relatable to particle size distribution.

In Section 2 of this report, we present, but do not show the derivation of, the equations that describe the two kinds of scattering processes, and present a model of the "turbulent" dielectric fluctuations that we believe will simulate the conditions at a mixing interface between

dust-laden and clean air. Section 3 presents dust particle size density distribution data obtained from aircraft flights through the "Middle Gust-Mixed Company" test dust cloud. From this data, we developed a size distribution model for use in our comparisons.

In Section 4, we use the information in Sections 2 and 3 for quantitative comparisons. We consider both our "Middle Gust-Mixed Company" dust model and unlikely particle size distributions that favor coherent scattering. Section 4 also summarizes our scattering equations. Section 5 presents our conclusions.

2. SCATTERING FORMULAS

Here we define our terminology and present analytical results. Let the probability that a particle has a radius between a and a + da be given by the function p(a). Then the following is true:

$$\int_{o}^{\infty} p(a)\ da = 1. \tag{1}$$

We shall assume that the particle-size probability-density distribution function p(a) is not a function of position $\vec{x}$. Let the number of particles/cm^3 at position $\vec{x}$ be $n(\vec{x})$. Usually, the number of particles/cm^3 is not available. The mass density of dust added to the atmosphere is more often provided. This mass density is given by:

$$m(\vec{x}) = n(\vec{x}) \int_{a=o}^{\infty} p(a)\ \frac{4\pi}{3}\ \rho_d\ a^3 da \tag{2}$$

In this equation, spherical particles are assumed; ρ_d is the density of the material of which the particles are made. For example, ρ_d for water droplets would be about 1.0. The dust particles we are concerned with often have a $\rho_d \simeq 2.0$.

The scattering of radar signals from the particles will be described by a two-region model. In the small particle size region, the cross section is given by the Rayleigh scattering cross section. For our study, this cross section is given adequately as:

$$\sigma(a,\lambda) = 4\pi a^2\ (ka)^4 \qquad a \ll \lambda \tag{3}$$

For simplicity, we assume that the particulate dielectric constant is significantly greater than 1.0.* The quantity λ is the radar wavelength, and $k = 2\pi/\lambda$. When the particle becomes large compared to a wavelength, then the radar cross section is geometric; this cross section is given as:

$$\sigma(a,\lambda) = \pi a^2 \qquad a \gg \lambda \tag{4}$$

We would normally assume that the transition from one region to the other takes place at a transition particle radius given by:

$$a_t = \frac{\lambda}{2\pi\sqrt{2}} . \tag{5}$$

In fact, for most of the work presented in this section, the radar wavelength is so much larger than most of the dust particle radii that we will safely assume a scattering cross section as given by Eq (3). [In later sections we shall use the two-region cross section formalism described by Eqs (3) through (5)]. The scattering per unit volume by the incoherent process is given by:

$$\sigma_I = \bar{n} \int_0^\infty p(a)\sigma(a,\lambda)da . \tag{6}$$

The quantity $\bar{n}$ is the expectation particle number density (number/cm^3). The semicoherent scattering cross section per unit volume is given by:

$$\sigma_c = \overline{\Delta n^2} \left[\int_0^\infty p(a) \sqrt{\sigma(a,\lambda)}\, da \right]^2 (2\pi)^3 \, \delta_3(2k_x,0,0) . \tag{7}$$

---

* The missing factor that multiplies Eq (3) is $\left|\frac{\epsilon - 1}{\epsilon + 2}\right|^2$. For our work with the ratio of coherent to incoherent scatter, this term cancels.

In this equation, $\overline{\Delta n^2}$ is the variance in fluctuations in particle number density. The integral, in essence, sums the scattering amplitudes of the individual particles. The scattering amplitude is taken as the square root of the particle cross section. The quantity ξ_3 is the in-situ three-dimensional spatial frequency power spectrum of dust density fluctuations. In Eq.(7), we assume that the radar beam travels along the x axis. The power spectrum is evaluated at $k_y = k_z = 0$. The x value is shown as $2\,k_x$ where $k_x = \frac{2\pi}{\lambda}$. This power spectrum is defined as the Fourier transform of the three-dimensional spatial correlation function for density fluctuations. This correlation function is normalized to have a value of 1.0 at 0 spacing and a value of 0 at very large spacing. We note that in the Rayleigh region the quantity $\sqrt{\sigma(a,\lambda)}$ is proportional to a^3, so the integral in Eq.(7) is proportional to mass density as given by Eq.(2).

Our discussion is really concerned with the ratio of coherent scatter to incoherent scatter. This ratio is given by:

$$\frac{\sigma_c}{\sigma_I} = \frac{\overline{\Delta n^2}}{\bar{n}^2}\ \bar{m}\left(\frac{3}{4\pi\rho_d}\right)\frac{\overline{a^3}}{\overline{a^6}}\ (2\pi)^3\ \xi_3(2k_x,0,0).^{*} \qquad (8)$$

We have written the ratio in this manner to emphasize quantities either that our intuition can relate to or that are measured in field experiments. The first quantity, $\overline{\Delta n^2}/\bar{n}^2$ is the square of the fractional density fluctuations. This quantity is sometimes referred to as the square of the condensation ratio, or simply as the condensation ratio. The quantity $\bar{m}$ is the expectation mass density in g/cm^3. The quantities $\overline{a^3}$ and $\overline{a^6}$ are the appropriate moments of the particle size distribution.

---

* The ratio $\overline{a^3}\ /\ \overline{a^6}$ used here ignores the transition from the Rayleigh scattering cross section to geometric. In our numeric results presented in Section 4, we use the two-region description.

To evaluate the importance of coherent scattering phenomena relative to that of incoherent backscattering, we will have to estimate the various quantities in Eq. (8). To the best of our knowledge, there have been no measurements of the condensation ratio. During the early stages of high-explosive-produced dust clouds, dust-laden air probably encircles clean air, in which case the condensation ratio will have a large value, perhaps approaching 1.0. As time progresses, the dust diffuses and turbulent mixing enhances this diffusion, so we assume that the condensation ratio decreases to significantly smaller values. This ratio ought to be largest near the edges of dust clouds, where dust-laden vortex rings mix with clean air.

The quantity $\bar{m}$, the average dust density in the dust cloud, was measured in field experiments and found to have values as high as several times $10^{-3}/cm^3$ to values below 10^{-8} g/cm^3. We shall investigate this below.

For our work here, we shall assume that $\rho_d = 2$ g/cm^3 (125 lbs/ft^3). The ratio of the third moment to the sixth moment of the dust-particle size distribution is discussed in Section 3. Data that permit us to accurately estimate this ratio are extremely sketchy.

Our concern is with dust mixing in an isotropic, turbulent medium. Under these circumstances, it is traditional to assume that the power spectrum, Φ_3, is given by the Kolmogorov spectrum. It is also traditional to assume that the relevant part of that spectrum is the inertial subrange in which the spectrum varies as given in Eq. (9).

$$\Phi_3(k) \propto (k)^{-11/3} \quad . \tag{9}$$

The form we will actually use is given in Eq. (10):

$$\Phi_3(\vec{k}) = \frac{b^3}{2\pi} \cdot \frac{(2p - 3)\,\Gamma(p)}{\sqrt{\pi}\,\Gamma(p - \frac{1}{2})} \cdot \frac{1}{(1 + b^2\vec{k}^2)^p} \quad . \tag{10}$$

The quantity b, which is a linear distance in centimeters, is traditionally chosen to be about the size of the input eddies. Traditionally one chooses a value for b on the order of 1/10 the scale of the hydrodynamic turbulent region. According to Eq. (10), we should use a value of $p = \frac{11}{6}$. However, if we choose a value of $p = 2$, the result will be very close to that of Eq. (9); furthermore, real-world experiments find values of p that range from 11/6 to 3.5. Finally, by assuming a value of 2 for p, the derived one-dimensional spectrum is proportional to k^{-2}, a value consistent with the spectrum expected for two turbulent mixing media. We therefore feel justified in accepting the analytical simplicity of the result of using $p = 2$. When these concepts are all assembled, we obtain Eq. 11:

$$\frac{\sigma_c}{\sigma_I} = \frac{\overline{\Delta n^2}}{\bar{n}^2} \cdot \frac{\bar{m}}{\rho_d} \cdot \frac{\overline{a^3}}{\overline{a^6}} \cdot \frac{6b^3}{(1 + b^2k^2)^2} \quad . \tag{11}$$

The quantity b will take on values of about 100 m. In this equation, the value of k is chosen to be $\frac{4\pi}{\lambda}$. We are concerned with radar wavelengths, λ, of 1 m or less, so that b^2k^2 will be much more than 1. This leads us to Eq. (12), which is the scattering formula that we shall use for our comparisons:

$$\frac{\sigma_c}{\sigma_I} = \frac{\overline{\Delta n^2}}{\bar{n}^2} \cdot \frac{\bar{m}}{\rho_d} \cdot \frac{\overline{a^3}}{\overline{a^6}} \cdot \frac{6\lambda^4}{b(4\pi)^4} \quad . \tag{12}$$

The condensation ratio is not currently predictable from theory and we know of no measurements; we will leave it to be studied later as a free parameter. The moments of the dust particle size distribution are not well measured but some data are available. These are given in Section 3.

Note that we have assumed that the dust particle will flow without slip with the air turbulence. Actually, the heavier dust particles will be affected by both air flow and by gravity, so they may not mirror the turbulent spectrum of Eqs. (11) and (12). The net result of this is to reduce the real-world coherent scattering magnitude relative to the theoretical values that we present below.

3. CHOICE OF A DUST MODEL

A model of the dust-particle size distribution, p(a), needs to be developed to calculate the various moments used in the scattering theory. The most complete data that we now have available of measurements of particle size distribution are in Reference 1. Dust density and particle size distributions were measured by flying an airplane through various parts of the cloud several times following surface high-explosive detonations. Filters were used to collect particles, and microscopic examination and particle counting were used to determine size distributions. The experiment of Ref. 1 was very inefficient at collecting particles with radii below 10 microns. The smaller particles are more efficient at producing coherent scattering than are the larger particles. No one knows what the particle number density is at those smaller sizes. We therefore assume that our model will underestimate somewhat the contribution of the coherent scattering processes.

The Ref. 1 presents particle size data in two figures and in their text. Our Table 1 attempts to summarize our interpretation of their results. The article is not as clear on several points as we need. The experiment did not sample many airborne particles with diameters significantly greater than 1500 microns. Therefore, our modeling at larger sizes than this is an expedient that we use to force moment integrals to converge. In fact, the largest particle obtained was found in a fallout collection plate some 5000 ft from ground zero. This particle had a diameter of 7000 microns (7 mm).

The data in Table 1 give power law coefficients for two particle size regions designated "small size" and "large size." The small sizes sampled were larger than 10 microns, though the data actually presented

---

1. W. D. Green and P. McMurry, "Middle Gust-Mixed Company: Dust Characterization," Meteorology Research Inc. Paper contained in Mixed Company/Middle Gust Results meeting, 13-15 March 1973, Vol. 1, DNA-3151 P1, pp. 451-462 (UNCLASSIFIED).

showed data plotted down only to 30 or 40 microns in diameter. The power law coefficients are, of course, the exponent of a power law fit locally in the small size and large size regions. The density presented in the table was given by the authors based on counting particles and particle radii. Inasmuch as their filters did not collect particles below 10 microns in size, the actual dust densities may be greater.

Table 1

BRIEF SUMMARY OF DUST PARTICLE SIZE DATA

Time of Sample (min/sec)	Part of Cloud Sampled	Power-Law Coefficient			Dust Density g/cm^3	Largest Particle Shown in Data Sample (microns)
		Small Size	Transition Radius (microns)	Large Size		
1:34	Main cloud	-3.26	300	-6.45	$4 \cdot 10^{-7}$	550
2:40	Top of stem	-2.34	-	-4.39	$2.1 \cdot 10^{-7}$	-
4:20	Middle of stem	-3.75	600		$8 \cdot 10^{-8}$	-
6:30	Same altitude in stem as sampled at 4:20	-3.7	380	-9.8	$>8 \cdot 10^{-8}$	800

*Largest particle sampled anywhere outside crater ejecta fall-back zone had a diameter of 7000 microns (7 mm) and was collected in a "fall-out" tray 5000 feet from ground zero.

We are glossing over several anomalies in the data of Ref. 1. If dust modeling becomes more important, an effort should be made to obtain more recent and refined data.

As a result of studying these data, we have developed an analytical model for the function p(a). We note that the data of Table 1 vary significantly in time and place. Our model, given in Eq. (13) is an attempt to approximate the general features of the data of Table 1:

$$p(a) = \frac{12.1}{1 + \frac{a^3}{10^3} + \frac{a^6}{1.16 \times 10^{11}} + \frac{a^9}{5.78 \times 10^{21}}} \text{ (micron}^{-1}\text{)}. \quad (13)$$

In this expression, the radius, a, is expressed in microns. Our analytical model contains four power-law regions. At very low particle sizes, the power-law coefficient is zero. This covers radii smaller than measured in the experiments of Reference 1. At a 10-micron radius, the model transits to inverse $(\text{radius})^3$. At a 600-micron radius, the equation transits to an inverse $(\text{radius})^6$. At a 3000-micron radius, the model transits to inverse $(\text{radius})^9$. This latter choice is in order to make the sixth order moment integral coverage rapidly. Since there are no data in that size region, we have chosen this steep power law as an expedient in the absence of theoretical guidance. Figure 1 plots the function p(a) (unnormalized) from a radius of 0.1 microns up to 10,000 microns.

Table 2 presents various moments of the size distribution. The table shows that our model gives a mean radius of 9.8 microns. We also show the ratio of the third moment to sixth moment as used in Eqs. (11) and (12). In the next section, we modify this moment ratio according to the two-region scattering model discussed in Section 2 and its character for different size particle distributions.

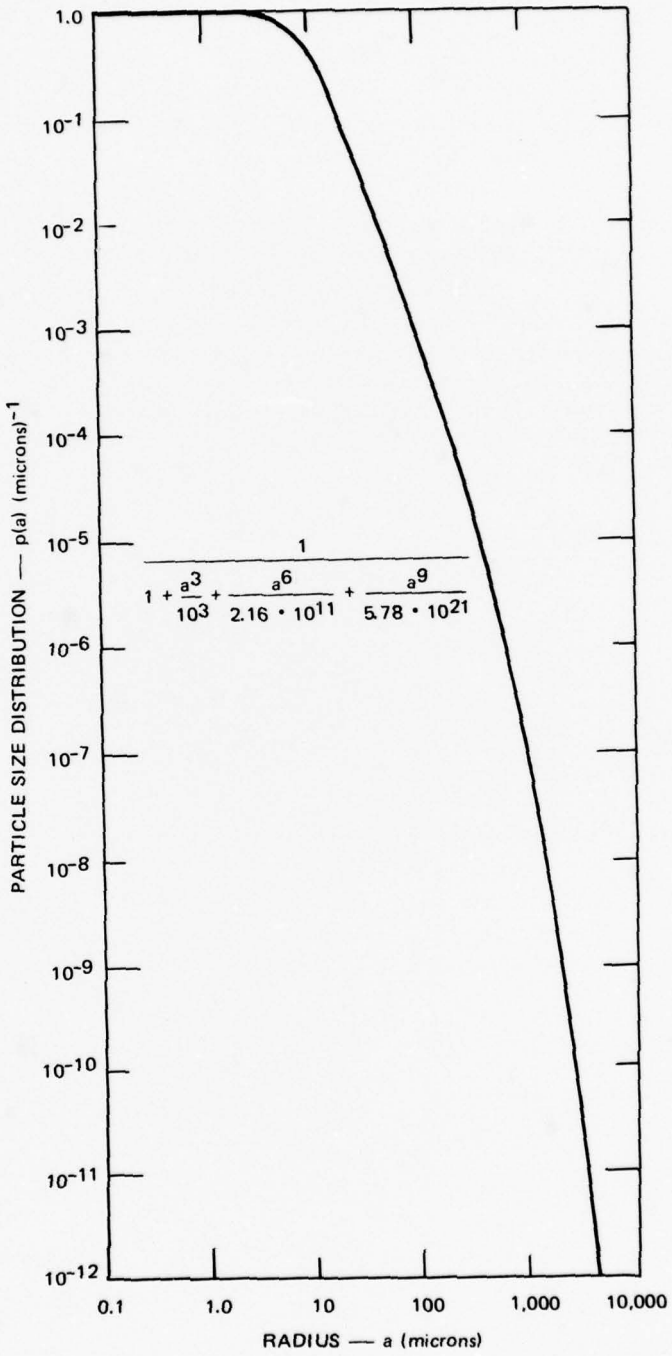

FIGURE 1 DUST PARTICLE SIZE DISTRIBUTION BASED UPON MIDDLE GUST-MIXED COMPANY MEASUREMENTS

Table 2

VARIOUS MOMENTS OF PARTICLE SIZE
DISTRIBUTION GIVEN BY EQUATION (13) AND
DISPLAYED BY FIGURE 1

Moment Designation	Value in Micron Measure	Value in Centimeter Measure
$\overline{a^1}$	9.81 micron	$9.81 \cdot 10^{-4}$ cm
$\overline{a^3}$	$5.72 \cdot 10^{4}$ (microns)^3	$5.72 \cdot 10^{-8}$ (cm)^3
$\overline{a^6}$	$5.23 \cdot 10^{13}$ (microns)^6	$5.23 \cdot 10^{-11}$ (cm)^6
$\dfrac{\overline{a^3}}{\overline{a^6}}$		$1.09 \cdot 10^{3}$ (cm)$^{-3}$

4. QUANTITATIVE STUDY OF COHERENT VS INCOHERENT SCATTER

Section 2 presented the scattering ratio formula. We indicated there that the ratio of coherent to incoherent scattering from particulate clouds depends on the ratio of moments of the particle size distribution. In this section we present some numerical examples that demonstrate the effect of this moment ratio.

According to the scattering cross section model presented in Section 2, particles that were small compared to a wavelength experienced Rayleigh scattering; large particle scattering was described by a geometric cross section. Figure 2 presents frequency versus transition radius in microns. Particle radius/frequency combinations below and to the left of the diagonal line we describe by the Rayleigh cross section. Combinations to the upper right we describe by a geometric cross section. We stated in Section 2, that dielectric properties would be ignored by assuming that the dielectric constant was much greater than 1. In fact, in the ratio calculations the dielectric constant term cancels, so that the value of the dielectric constant is not relevant.

We shall first consider particulate clouds with a single size particle. Table 3 presents data on various moment ratios for our dust model of Section 3 and for single size particle distributions. Actually, the factors of Table 3 are to be used in connection with Eq. (15) below. The scattering moment ratio, which is nearly $\overline{a^3} / \overline{a^6}$ if particles are very small compared to wavelength, is given in Table 3 for 1-micron through 300-micron size particles. Referring back to Eq. (12), we see that, for a given mass density and a given condensation ratio, if the cloud is made of 1-micron particles, the ratio of coherent to incoherent scattering will be 1 million times greater than if all the particles have radii of 100 microns. Rain drops characteristically have radii in excess of 100 microns (0.1 m), so it is seldom expected that scattering from rainfall would contain coherent contributions. On the other hand, we see that scattering from extremely fine particulate matter could be totally

Table 3

SCATTERING MOMENT FACTORS FOR USE IN EQUATION 15

Dust Model (microns)	Frequency (MHz)	Numerical Factor for Eq.(15) (cm^{-3})	$\overline{a^3} / \overline{a^6}$ (cm^{-3})
Radius			
All 1	All	$1.20 \cdot 10^{8}$	10^{12}
All 10	All	$1.20 \cdot 10^{5}$	10^{9}
All 100	$<\sim 300{,}000$	$1.20 \cdot 10^{2}$	10^{6}
All 300	$< 100{,}000$	$4.46 \cdot 10^{0}$	$3.7 \cdot 10^{4}$
Continuous size distribution	10^{3}	$1.32 \cdot 10^{-1}$	$1.09 \cdot 10^{3}$
	$3 \cdot 10^{3}$	$1.35 \cdot 10^{-1}$	↓
	10^{4}	$1.71 \cdot 10^{-1}$	
	$3 \cdot 10^{4}$	$4.67 \cdot 10^{-1}$	
	10^{5}	$3.15 \cdot 10^{0}$	

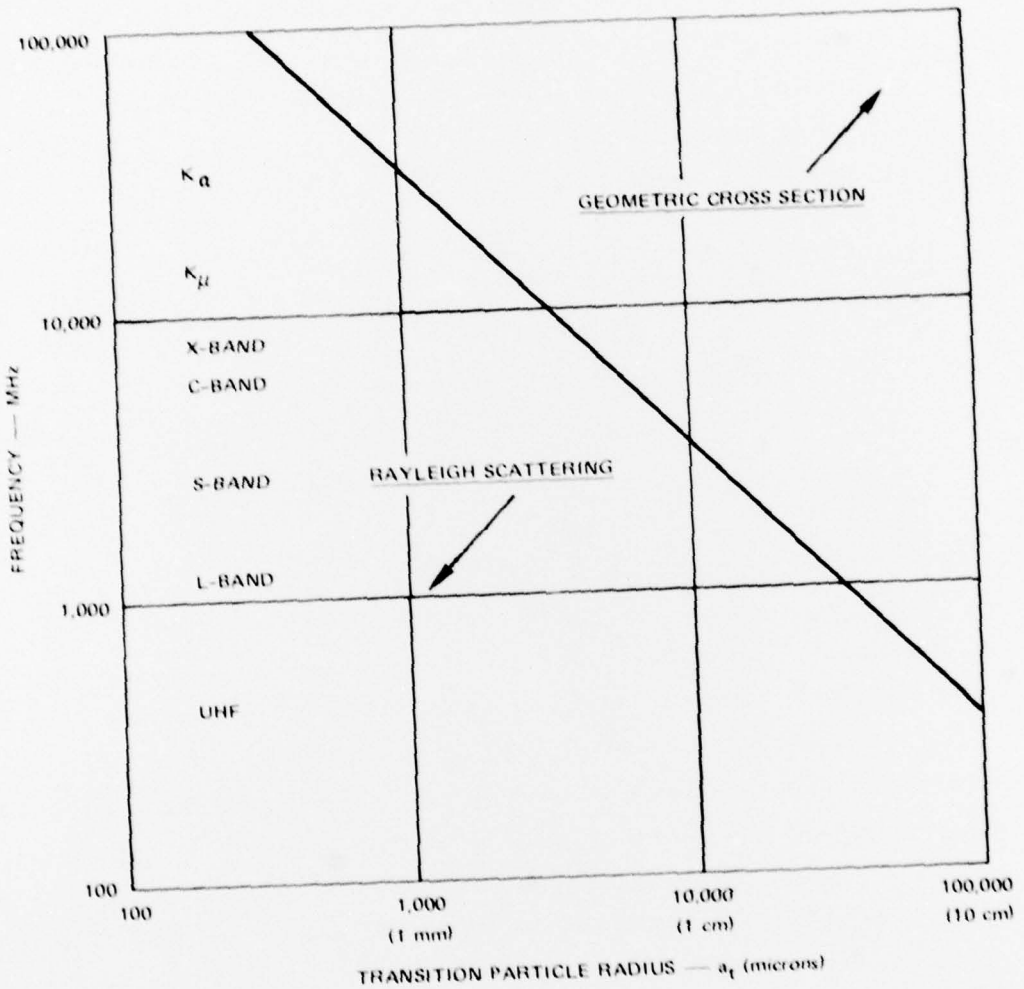

FIGURE 2 PARTICLE RADIUS FOR TRANSITION FROM RAYLEIGH TO GEOMETRIC CROSS SECTION

dominated by coherent scattering phenomena. Electrons, atoms, and molecules, where the effective radii are very small, are cases in point. Indeed coherent scattering in electron plasmas may exceed incoherent contributions by factors of 10^6 to 10^{10}.

In Section 2, where we described the scattering formulas, we assumed that the scattering cross section was Rayleigh over the entire particle size range. Our numerical answers presented below use the more complex scattering amplitude weighting formula that pertains for the Rayleigh and geometric regions. This expression is given by:

$$\frac{\sigma_c}{\sigma_I} = \frac{\overline{\Delta n^2}}{\bar{n}^2} \cdot \frac{\bar{m}}{\rho_d} \cdot \frac{6\lambda^4}{b(4\pi)^4} \cdot \frac{\left[\int_o^{a_t} p(a)a^3 da + \frac{1}{2}\left(\frac{\lambda}{2\pi}\right)^2 \int_{a_t}^{\infty} p(a)a\, da\right]^2}{\int_o^{\infty} p(a)a^3 da \left[\int_o^{a_t} p(a)a^6 da + \frac{1}{4}\left(\frac{\lambda}{2\pi}\right)^4 \int_{a_t}^{\infty} p(a)a^2 da\right]} \tag{14}$$

Equation (15) separates Eq. (14) into factors to be chosen and a factor that we have presented in Table 3. The table shows the ratio of 3rd to 6th moments for our dust model, which, of course, does not depend on radar frequency. For our dust model, we see that at frequencies above 10,000 MHz the two-region scattering model must be used, since significant contributions to scattering came from particles that are larger than the transition radius. The effect of having some particles in the geometric cross section region is to enhance coherent effects compared with incoherent scattering, but both scattering processes are reduced over what would pertain for Rayleigh scattering only.

$$\frac{\sigma_c}{\sigma_I} = 2 \frac{\overline{\Delta n^2}}{\bar{n}^2} \cdot \frac{\bar{m}}{\rho_d} \cdot \frac{\lambda^4}{b} \cdot \text{(factor from Table 3)} \tag{15}$$

As a basis for comparison, we present in Figure 3 the various cross sections per unit volume for an air-laden dust density of $10^{-7}/cm^3$ with a dust material density of 2.0. Figure 3 shows incoherent scattering cross section vs frequency for our continuum particle size model, expressed earlier in Eq. (13) and Figure 1. We also show the volume scattering cross section for dust particle clouds in which the particles are all the same size.

The coherent scattering cross section for the same density parameters and a condensation ratio $\overline{\Delta n^2} / \bar{n}^2 = 1$, a turbulent input eddy size of 100 meters (b = 100 meters) are also shown. The input eddy size of 100 m is only a guess that is ~ 1/10th the cloud vortex ring diameter.

Coherent scattering from a dust-particle size distribution, as we presented earlier, tends to decrease at high frequencies, as does the incoherent scattering, because the larger particles become part of the geometric scattering cross-section region. If all particles were in the Rayleigh region, then the coherent scattering would be frequency independent, would not depend on particle size distribution, and would only depend on the total dust density fluctuations at the appropriate spatial wavelengths.

The data presented by Robbiani[2] are very difficult to decipher in terms useful to us. But we deduced that his measurements would be like those indicated at a volume scattering of $10^{-6}\ m^2/m^3$.

At the dust level values that we have chosen, coherent scattering seems unimportant. Figure 4 presents the ratio of coherent to incoherent scattering versus frequency for two levels of air-laden dust density, 10^{-3} and 10^{-7} per cm^3. This range probably spans most densities of concern to us. These curves are for our continuous particle size dust model. If we had wished to use single size particles, say if all particles had radii of 10 microns (an improbable natural distribution) then we might have found that coherent scattering effects would be important. This result is readily deduced from Figure 3.

---

2. R. L. Robbiani, "Middle North Series Mixed Company Event, X-Band Radar Reflectivity," Fort Monmouth, New Jersey, POR 6616, 23 July 1973, (UNCLASSIFIED).

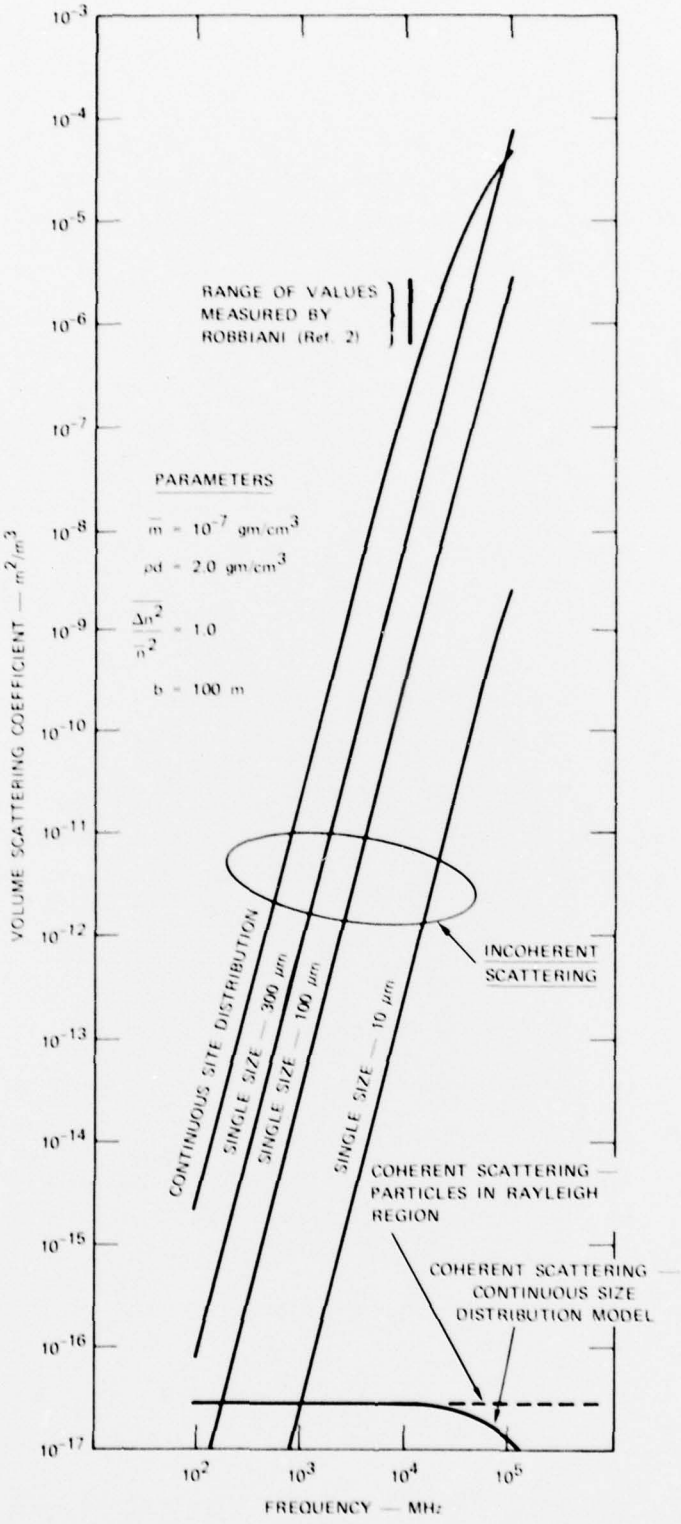

FIGURE 3 VOLUME SCATTERING COEFFICIENT vs RADAR FREQUENCY FOR VARIOUS DUST PARTICLE SIZE DISTRIBUTIONS, INCOHERENT AND SEMICOHERENT SCATTERING

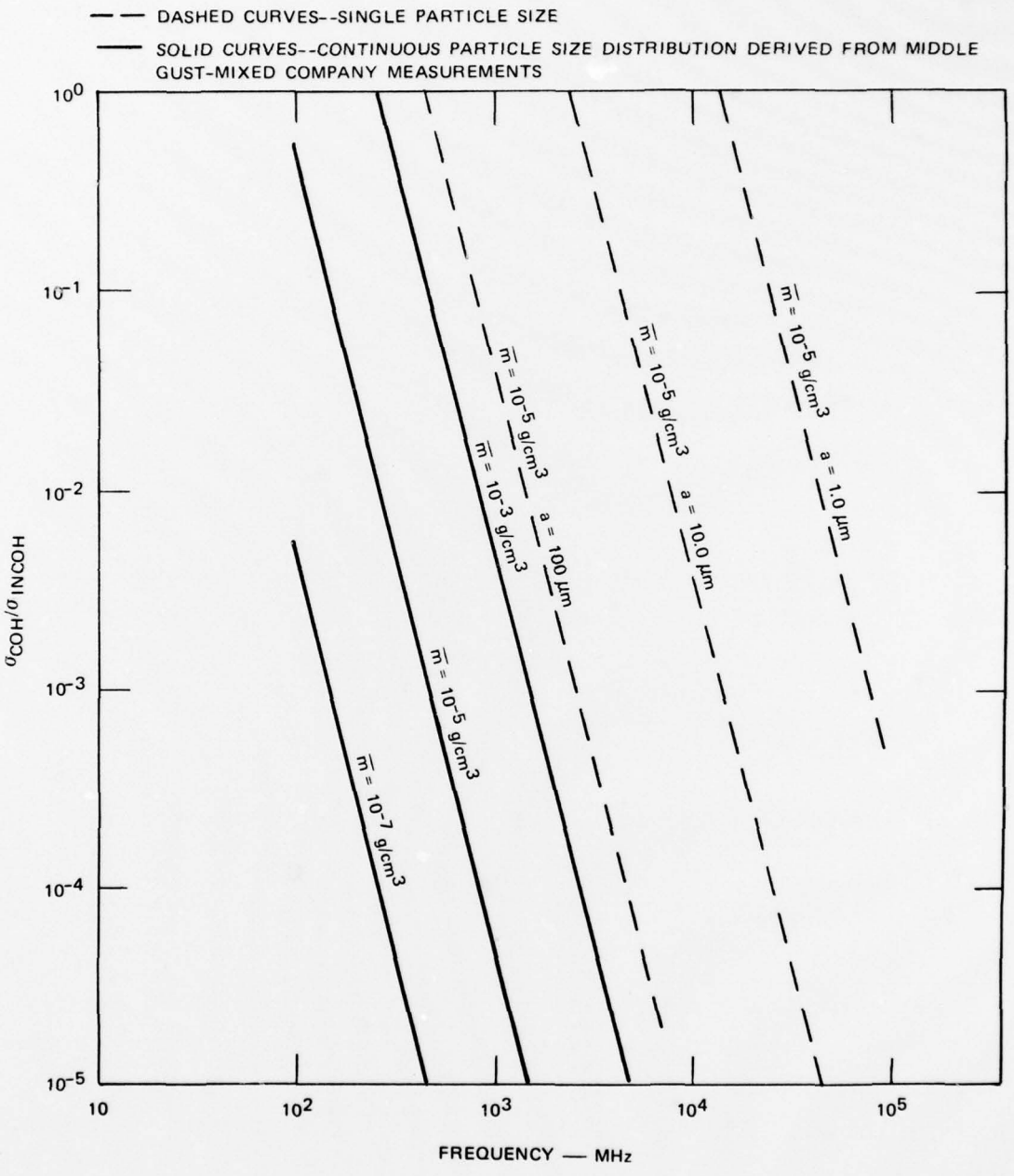

FIGURE 4 RATIO OF COHERENT TO INCOHERENT SCATTERING vs RADAR FREQUENCY FOR VARIOUS MODELS OF DUST PARTICLE SIZE DISTRIBUTION

Equation 16 presents the incoherent volume-specific scattering cross section for our two-region particle scattering model. The expression a_t is the transition radius between Rayleigh and geometric scattering.

$$\sigma_I = \frac{\bar{m}}{\rho_d} \cdot \frac{6(2\pi)^4}{\lambda^4} \left[\frac{\int_o^{a_t} p(a) a^6 da + \frac{\lambda^4}{4(2\pi)^4} \int_{a_t}^{\infty} p(a) a^2 da}{\int_o^{\infty} p(a) a^3 da} \right] \tag{16}$$

If all particles were of the same size (unlikely) and in the Rayleigh region, then the incoherent cross-section could be found by:

$$\sigma_I = \frac{\bar{m}}{\rho_d} \frac{6(2\pi)^4}{\lambda^4} \cdot a^3 . \tag{17}$$

Equation 18 presents the volume-specific radar cross section for coherent scattering from a turbulent dust cloud using our model of the turbulent spectrum and the two-region scattering model.

$$\sigma_c = \frac{\overline{\Delta n^2}}{\bar{n}^2} \cdot \frac{\bar{m}^2}{\rho_d} \cdot \frac{1}{b} \cdot \frac{9}{8} \left[\frac{\int_o^{a_t} p(a) a^3 da + \int_{a_t}^{\infty} p(a) a \, da}{\int_o^{\infty} p(a) a^3 da} \right]^2 \tag{18}$$

Equation 19 represents coherent scattering when all particles are in the Rayleigh region. Note that under this condition the coherent cross section depends only on the density of dust in the air. Particle size does not matter. Our model for $\Phi_3(\vec{k})$ leads to a result that is frequency-independent.

$$\sigma_c = \frac{\overline{\Delta n^2}}{\bar{n}^2} \cdot \frac{\bar{m}^2}{\rho_d^2} \cdot \frac{1}{b} \cdot \frac{9}{8} \tag{19}$$

5. CONCLUSIONS

Results of our calculations have been used to compare the intensity of coherent scattering from density fluctuations in dust clouds with the intensity of incoherent scattering. The calculations were made using a model of the spectrum of density fluctuations that is consistent with that expected from turbulent mixing theory. The principal results of our study are:

(1) The incoherent scattering cross section per unit volume depends upon the details of the particle size distribution.

(2) The coherent scattering cross section *does not* depend on the particle size distribution if the largest particles are small enough to be in the Rayleigh region.

(3) The coherent scattering cross section depends on the square of the air-laden dust density; incoherent scattering depends linearly on this density.

(4) For a reasonable choice of dust-particle size distribution, air-laden dust densities (appropriate to later-time dust clouds), an acceptable model of turbulent structure, and an over-estimate of the dust density condensation ratio, coherent scattering is weaker than incoherent scattering, except at the very lowest radar frequencies.

The above conclusions are based on the assumption that dust particles exactly follow air particles. Since the heavier dust particles are also affected by gravity, they will not exactly follow air motion and so will not mirror small-scale air turbulence fluctuations. The result is a further reduction of coherent scattering compared with our predictions.

If one postulates unphysical dust-particle size distributions (for example, that all particles are below 10 microns in diameter) and large air-laden dust density (greater than $\sim 10^{-3}$ g/cm^3), then coherent

scattering can be greater than incoherent scattering at the lower radar frequencies. In a sense this is exactly the situation for electrons scattering in turbulent reentry wakes and for scattering that can be obtained from hot and cold (or dry and moist) turbulent mixing air. In these circumstances, the particles are electrons and molecules, respectively, and the scattering can be studied as mixtures of individual particles, which is how we studied dust. However, we customarily handle these latter environments in terms of their aggregate properties expressed in terms of the medium's dielectric constant.

Our most important finding, though, is that interpretation of multifrequency radar scattering measurements in dust clouds obtained using scaled beamwidths does not require consideration of semicoherent, scattering from turbulent mixing of clean and dirty air, especially for radar frequencies greater than 1000 MHz.

DISTRIBUTION LIST

DEPARTMENT OF DEFENSE

Assistant Secretary of Defense
Comm, Cmd, Cont, & Intell.
ATTN: M. Epstein
ATTN: J. Babcock

Assistant to the Secretary of Defense
Atomic Energy
ATTN: Executive Assistant

Command & Control Technical Center
Department of Defense
ATTN: C-312, R. Mason

Defense Advanced Rsch. Proj. Agency
ATTN: TIO

Defense Communications Agency
ATTN: Code 101B
ATTN: Code 480

Defense Communications Engineer Center
ATTN: Code R410, J. McLean

Defense Documentation Center
12 cy ATTN: DD

Defense Nuclear Agency
ATTN: DDST
3 cy ATTN: SPAS, T. Hopkins
4 cy ATTN: TITL
4 cy ATTN: RAAE

Field Command
Defense Nuclear Agency
ATTN: FCPR

Field Command
Defense Nuclear Agency
Livermore Division
ATTN: FCPRL

Interservice Nuclear Weapons School
ATTN: TTV

Joint Chiefs of Staff
ATTN: J-3, WWMCCS Evaluation Office

National Security Agency
ATTN: R52, J. Skillman

Under Secy. of Def. for Rsch. & Engrg.
Department of Defense
ATTN: Strategic & Space Systems (OS)

WWMCCS System Engineering Org.
ATTN: R. Crawford

DEPARTMENT OF THE ARMY

Atmospheric Sciences Laboratory
U.S. Army Research & Development Command
ATTN: DELAS-BL-D, H. Holt
ATTN: DELAS-EO, F. Niles
ATTN: DELAS-EO, D. Snyder

DEPARTMENT OF THE ARMY (Continued)

BMD Advanced Technology Center
Huntsville Office
Department of the Army
ATTN: ATC-R, D. Russ
ATTN: ATC-T, M. Capps
ATTN: ATC-O, W. Davies

Harry Diamond Laboratories
Department of the Army
ATTN: DELHD-N-TI, M. Weiner
ATTN: DELHD-N-NP, F. Wimenitz

U.S. Army Foreign Science & Tech. Ctr.
ATTN: DRXST-SD
ATTN: R. Jones

U.S. Army Materiel Dev. & Readiness Cmd.
ATTN: DRCLDC, J. Bender

U.S. Army Missile Intelligence Agency
ATTN: J. Gamble

U.S. Army Missile R&D Command
ATTN: Document Section
ATTN: DRDMI-XS

U.S. Army Nuclear & Chemical Agency
ATTN: Library

U.S. Army Satellite Comm. Agency
ATTN: Document Control

U.S. Army TRADOC Systems Analysis Activity
ATTN: ATAA-SA

Project Manager, Smoke
ATTN: T. Vandewal

DEPARTMENT OF THE NAVY

Naval Electronic Systems Command
ATTN: Code 5011
ATTN: PME 117-T

Naval Research Laboratory
ATTN: Code 7555
ATTN: Code 2627
ATTN: Code 7551
ATTN: Code 6730, E. McClean
ATTN: Code 6701, J. Brown
ATTN: Code 6700, T. Coffey

Naval Surface Weapons Center
ATTN: Code F-14, R. Butler

Office of Naval Research
ATTN: Code 465

Strategic Systems Project Office
Department of the Navy
ATTN: NSP-2722, F. Wimberly
ATTN: NSP-2141

DEPARTMENT OF THE NAVY (Continued)

Naval Surface Weapons Center
White Oak Laboratory
ATTN: Code F31

DEPARTMENT OF THE AIR FORCE

Aerospace Defense Command
Department of the Air Force
ATTN: DC, Mr. Long

Aerospace Defense Command
ATTN: XPDQQ

Air Force Avionics Laboratory, AFSC
ATTN: AAD, W. Hunt
ATTN: AAD, A. Johnson

Air Force Geophysics Laboratory, AFSC
ATTN: OPR-1, J. Ulwick
ATTN: OPR, H. Gardner
ATTN: LKB, K. Champion
ATTN: OPR, A. Stair
ATTN: PHD, J. Buchall
ATTN: PHD, J. Mullen

Air Force Weapons Laboratory, AFSC
ATTN: SUL
ATTN: CA
ATTN: DYC, J. Kamm
ATTN: DES, G. Ganong
ATTN: DYC, J. Barry

Deputy Chief of Staff
Research, Development & Acq.
Department of the Air Force
ATTN: AFRDQ

Rome Air Development Center
ATTN: TSLD
ATTN: OCSE, V. Coyne

Space & Missile Systems Organization
Air Force Systems Command
ATTN: MNX

Space & Missile Systems Organization
Air Force Systems Command
ATTN: RSP

Space & Missile Systems Organization
Air Force Systems Command
ATTN: SKA, M. Clavin

Space & Missile Systems Organization
Air Force Systems Command
ATTN: SZJ

Strategic Air Command
ATTN: SPFS, B. Stephan
ATTN: NRT
ATTN: A. Bauer

OTHER GOVERNMENT AGENCIES

Department of Commerce
National Oceanic & Atmospheric Admin.
Environmental Research Laboratories
ATTN: D. Williams

OTHER GOVERNMENT AGENCIES (Continued)

Institute for Telecommunications Sciences
National Telecommunications & Info. Admin.
ATTN: W. Utlaut

NASA
Goddard Space Flight Center
ATTN: P. Corrigan

DEPARTMENT OF DEFENSE CONTRACTORS

Aerospace Corp.
ATTN: D. Olsen
ATTN: V. Josephson
ATTN: N. Stockwell
ATTN: A. Morse
ATTN: W. Grabowsky
ATTN: I. Garfunkel
ATTN: G. Anderson

Analytical Systems Engineering Corp.
ATTN: Radio Sciences

Berkeley Research Associates, Inc.
ATTN: J. Workman

Boeing Co.
ATTN: G. Keister

Brown Engineering Company, Inc.
ATTN: R. Deliberis
ATTN: N. Passino

Charles Stark Draper Lab., Inc.
ATTN: D. Cox
ATTN: J. Gilmore

EG&G, Inc.
Los Alamos Division
ATTN: J. Walker
ATTN: J. Fu
ATTN: J. Breedlove

Electrospace Systems, Inc.
ATTN: P. Phillips
ATTN: H. Logston

ESL, Inc.
ATTN: J. Marshall
ATTN: C. Prettie

General Electric Co.
Space Division
ATTN: M. Bortner
ATTN: R. Edsall

General Electric Co.
ATTN: G. Millman

General Electric Co.-TEMPO
Center for Advanced Studies
ATTN: W. McNamara
ATTN: W. Knapp
ATTN: T. Stevens
ATTN: M. Stanton
ATTN: D. Chandler
ATTN: DASIAC

DEPARTMENT OF DEFENSE CONTRACTORS (Continued)

General Research Corp.
Santa Barbara Division
ATTN: J. Garbarino
ATTN: J. Ise, Jr.

Geophysical Institute
University of Alaska
ATTN: T. Davis
ATTN: N. Brown
ATTN: Technical Library

GTE Sylvania, Inc.
Electronics Systems Grp.-Eastern Div.
ATTN: M. Cross

HSS, Inc.
ATTN: D. Hansen

Information Science, Inc.
ATTN: W. Dudziak

Institute for Defense Analyses
ATTN: E. Bauer
ATTN: J. Bengston

JAYCOR
ATTN: S. Goldman

Johns Hopkins University
Applied Physics Lab.
ATTN: Document Library
ATTN: T. Potemra

Kaman Sciences Corp.
ATTN: N. Beauchamp
ATTN: T. Meagher
ATTN: F. Foxwell

Lawrence Livermore Laboratory
University of California
ATTN: L-31, R. Hager
ATTN: L-96, T. Donich
ATTN: L-389, R. Ott

Lockheed Missiles & Space Co., Inc.
ATTN: D. Churchill

Lockheed Missiles and Space Co., Inc.
ATTN: R. Au
ATTN: R. Johnson

Los Alamos Scientific Laboratory
ATTN: R. Taschek
ATTN: J. Zinn
ATTN: J. Malik
ATTN: E. Jones

M.I.T. Lincoln Lab.
ATTN: J. Evans
ATTN: D. Towle

Martin Marietta Corp.
Orlando Division
ATTN: R. Heffner

McDonnell Douglas Corp.
ATTN: W. Olson
ATTN: G. Mroz
ATTN: R. Halprin

DEPARTMENT OF DEFENSE CONTRACTORS (Continued)

Mission Research Corp.
ATTN: W. Crevier
ATTN: P. Fischer
ATTN: M. Scheibe
ATTN: S. Gutsche
ATTN: F. Fajen
ATTN: W. Schlueter
ATTN: C. Longmire
ATTN: R. Kilb
ATTN: D. Sowle
ATTN: R. Bogusch
ATTN: R. Hendrick
ATTN: D. Sappenfield

Mitre Corp.
ATTN: W. Foster
ATTN: W. Hall
ATTN: J. Wheeler

Photometrics, Inc.
ATTN: I. Kofsky

Physical Dynamics, Inc.
ATTN: A. Thompson

Physical Dynamics, Inc.
ATTN: E. Fremouw

R & D Associates
ATTN: W. Karzas
ATTN: F. Gilmore
ATTN: C. MacDonald
ATTN: B. Gabbard
ATTN: R. Lelevier
ATTN: H. Ory
ATTN: R. Turco

Rand Corp.
ATTN: E. Bedrozian
ATTN: C. Crain

Raytheon Co.
ATTN: G. Thome

Riverside Research Institute
ATTN: V. Trapani

Sandia Laboratories
ATTN: C. Mehl
ATTN: C. Williams
ATTN: 3141
ATTN: W. Brown
ATTN: T. Wright
ATTN: D. Thornbrough

Science Applications, Inc.
ATTN: D. Hamlin
ATTN: J. McDougall
ATTN: C. Smith
ATTN: L. Linson
ATTN: R. Lee
ATTN: D. Sachs

Science Applications, Inc.
Huntsville Division
ATTN: D. Divis

DEPARTMENT OF DEFENSE CONTRACTORS (Continued)

Science Applications, Inc.
ATTN: J. Cockayne

Space Data Corp.
ATTN: E. Allen

SRI International
ATTN: W. Jaye
ATTN: M. Baron
ATTN: C. Rino
ATTN: G. Smith
ATTN: J. Depp
ATTN: A. Burns
ATTN: W. Chesnut
ATTN: R. Leonard
ATTN: R. Leadabrand
ATTN: L. Cobb

DEPARTMENT OF DEFENSE CONTRACTORS (Continued)

SRI International
ATTN: F. Perkins

Technology International Corp.
ATTN: W. Boquist

TRW Defense & Space Sys. Group
ATTN: R. Plebuch

Visidyne, Inc.
ATTN: C. Humphrey
ATTN: J. Carpenter